Available online at www.sciencedirect.com
SCIENCE DIRECT®
International Journal of Heat and Mass Transfer 47 (2004) 959–968
International Journal of HEAT and MASS TRANSFER
www.elsevier.com/locate/ijhmt

Statistical treatment of scalar transfer in isotropic turbulence

Iwao Hosokawa *

Professor Emeritus, University of Electro-Communications, 2-24-6-101 Honmachi, Fuchu, Tokyo 183-0027, Japan

Received 19 August 2002; received in revised form 16 August 2003

Abstract

It has recently been known that local high-gradient regions of an advected scalar, such as temperature or mass contaminant, in a turbulent state of fluid form thin sheets, randomly oriented and moving around with turbulent motion. Here is presented a joint multifractal model for velocity and scalar dissipations in isotropic turbulence which can predict the statistical distributions of the worms, vorticity-concentrated regions, as well as the above-described scalar-gradient sheets. This model allows us to derive turbulent diffusion coefficient in isotropic turbulence scaled by Reynolds number and Prandtl number, which predominates far over molecular diffusion coefficient.

Keywords: Isotropic turbulence; Multifractal (intermittency) model; Tetranomial Cantor set; Advected scalar transfer; Scalar-gradient sheet; Turbulent Nusselt number

1. Introduction

One of the most important problems in turbulence theory is the process of turbulent mixing. This problem affects many industrial and ecological topics, in which we desire to know the heat or mass diffusion rate and sometimes the chemical reaction rate during turbulence. In order to discuss this process in detail, however, we need to know the expectedly universal, statistical structure of an advected scalar distributed in a turbulent fluid. Although many theoretical and experimental works on the structure functions of a passive scalar as well as the probability density functions (PDF) of its increment and gradient in a turbulent fluid have been published so far, the instantaneous morphologic feature of an advected scalar has not been researched very well. A reliable theory for explaining it is still lacking. Here is presented a bold but simple phenomenological method for investigating the statistical nature of the morphologic feature to be seen in isotropic turbulence on the basis of a joint scale-similar multifractal theory of dissipations of velocity and a passive scalar.

Now that we know that many worms, recognized as locally vorticity-concentrated slender regions in the flow, appear in isotropic turbulence in a statistically universal way, we may expect some kind of structure of a scalar advected in the isotropically turbulent flow to appear as well. According to the recent direct numerical simulation (DNS) of three-dimensional (3D) decaying isotropic turbulence with a passive scalar for Taylor-scale Reynolds number $R_\lambda = 160$ and Prandtl number $Pr = 1$ [1], we have recognized that many sheet-like regions with locally high values of scalar-gradient move around randomly in fully-developed turbulence. The thickness of the sheet is of the order-of-magnitude of Kolmogorov length $\eta\ (= (\nu^3/\varepsilon)^{1/4}$; ν: kinematic viscosity of fluid; ε: globally averaged energy dissipation rate per unit mass), while the width can reach integral scale L, at most, but the core part of the sheet which is really flat is considered as Taylor-scale wide on the average. The same feature was also evidenced by another DNS of forced isotropic turbulence with a passive scalar with a fixed mean scalar gradient for $R_\lambda = 88$ and $Pr = 0.7$ [2]. The previous DNS for $R_\lambda = 60$ and 45 by Ruetsch and Maxey [3,4], who also treated a forced isotropic turblence with a passive scalar with a fixed mean scalar gradient, are quite consistent with the above-described observations. In particular, their result suggests that the sheet lies on a local

* Tel.: +81-042-361-6450.
E-mail address: ihsk@coral.ocn.ne.jp (I. Hosokawa).

0017-9310/$ - see front matter © 2003 Elsevier Ltd. All rights reserved.
doi:10.1016/j.ijheatmasstransfer.2003.08.027

Nomenclature

C	constant of integration of Eq. (2); equal to S/d
d	thickness of a scalar-gradient sheet
L	macroscale length or integral scale
m_s	normalized thickness; d/η_s
$N(d)$	number of sheets with thickness d within the volume of L^3
N_{T}	total number of sheets in a macroscale box of volume L^3
Nu	Nusselt number
Pr	Prandtl number; ν/κ
$P(\ )$	PDF of the argument in the parenthesis
$p(y,z;r/l)$	PDF of y and z for scale ratio r/l
Re	macroscale Reynolds number
R_λ	Taylor-scale Reynolds number
r'	smallest scale over which we can consider the local character of turbulence, fully containing the inertial range
S	scalar gap across a scalar-gradient sheet
T	passive scalar
Tr	total transfer rate of passive scalar in a macroscale cube
t	time variable
u_j	jth component of velocity vector
$\langle u^2\rangle$	square-average of longitudinal velocity fluctuation
x_j	jth component of displacement vector
y	multiplier of energy dissipation; $\varepsilon_r/\varepsilon_l$
z	multiplier of scalar dissipation; χ_r/χ_l

Greek symbols

α	strain in the two-dimensional stagnant flow
δ	boundary layer thickness at distance x from the leading edge
ε	energy dissipation averaged over a macroscale cube; equal to ε_L
ε_r	energy dissipation averaged over a domain of scale r
η	Kolmogorov scale; $(\nu^3/\varepsilon)^{1/4}$
η_s	$(\kappa^3/\varepsilon)^{1/4}$
η_s'	local value of η_s in a domain of scale r'; $(\kappa^3/\varepsilon_{r'})^{1/4}$
κ	molecular diffusion coefficient of the passive scalar
κ_T	turbulent diffusion coefficient
λ	Taylor-microscale
λ'	local Taylor-microscale in a domain of scale r'
μ	second-order intermittency exponent
ν	kinetic viscosity
Σ	normalized scalar gap; $S/(\kappa^{1/4}\chi_L^{1/2}/\varepsilon_L^{1/4})$
χ_d	scalar dissipation at the middle of a scalar-gradient sheet
χ_r	scalar dissipation averaged over a domain of scale r

stagnation line with a persistent uniform strain, under the influence of some vortical structures in turbulence.

We have an exact steady solution of the advected scalar-gradient equation in the two-dimensional stagnant flow with a uniform strain, as is stated in the next section. This solution may be considered to give the approximative local structure of the above-described scalar-gradient sheet. This is similar to the situation where a Burgers vortex may approximate the vorticity field around a worm. Thus we can think of a random collection of many scalar-gradient sheets, each simulated by this steady solution, which are distributed in a turbulent fluid in accord with some universal statistics; just as we considered a collection of many Burgers vortices to approximate worms in real turbulence [5].

In the previous treatment of the statistics of worms in isotropic turbulence [5], we utilized the 3D binomial Cantor set model for energy dissipation measure [6] as a statistical device to link the instantaneous spatial arrangement of worms to the geometry of a universal scale-similar (dissipation) measure. Fortunately, we have developed a reasonable extension of this model to the case of turbulence with a passive scalar [7], what may be called the tetranomial Cantor set model for joint multifractal measure for energy and scalar dissipations. This can give rise to the anomalous scaling exponents of scalar structure functions [7], as well as to the PDF of scalar increment across various distances [8], both in excellent agreement with experiment in a way that this model is much better than the joint lognormal model proposed before. This fact suggests that there must be a self-similar structure of scalar dissipation measure as well. Therefore, it is natural and inevitable, at the present stage, to take this model as a base for considering the instantaneous spatial distribution of scalar-gradient sheets. Then we try to construct a phenomenological, statistical theory of the sheets on this basis, relying on another bold postulate which is finally stated in Section 3. The point of interest here is a possible way of characterizing statistical configuration of a collection of scalar-gradient sheets by a particular scale-similar measure (consistent with the DNS and experimental observations) and by the exact solution of a single sheet structure (described in next section).

In Section 4 the total characteristics of sheets in a macroscale cube are discussed to predict the turbulent

diffusivity in isotropic turbulence, which allows us to discuss the Nusselt number across a macroscale (nearly isotropic) turbulence box. We shall estimate the PDF of thickness, width of a sheet and that of scalar gap across a sheet in Appendix A and B. Our estimation may be too simple and still crude, but it is expected to help our systematic understanding of the statistical structure of scalar-gradient sheets in turbulence, at least until a more rigorous theory is established from the first principle on this matter.

2. Exact steady solution for a scalar-gradient sheet

As is well known, an advected scalar T is governed by

$$\partial T/\partial t + u_j \partial T/\partial x_j = \kappa \partial^2 T/\partial x_j \partial x_j, \tag{1}$$

where t is time variable, x_j and u_j represent the jth components of the vectors of position and velocity of the fluid flow, respectively, and κ is the diffusion coefficient of the scalar in fluid. The repeated subscripts imply the summation over them. Let us assume that the scalar depends only on x_1 and is in the two-dimensional stagnant flow with a uniform strain for which we have $u_1 = -\alpha x_1$, $u_2 = \alpha x_2$ and $u_3 = 0$. This stagnant flow is an exact solution of the Navier–Stokes equation. Then Eq. (1) becomes

$$\alpha x_1 \partial T/\partial x_1 + \kappa \partial^2 T/\partial x_1^2 = 0. \tag{2}$$

This allows $\partial T/\partial x_1$ to be solved exactly as

$$\partial T/\partial x_1 = C \exp[-\alpha x_1^2/(2\kappa)], \tag{3}$$

where C is a constant. Hence we have a solution for T as

$$T(x_1) = C \int_{-\infty}^{x_1} \exp\left(-\frac{\alpha x^2}{2\kappa}\right) \mathrm{d}x, \tag{4}$$

assuming that T vanishes as x_1 tends to $-\infty$. If we define the total scalar gap across the sheet as $S = T(\infty) - T(-\infty)$, then C is given as

$$C = S/(2\pi\kappa/\alpha)^{1/2}. \tag{5}$$

In view of the equation

$$[T(\infty) - T(-\infty)]/(\partial T/\partial x_1)_{\max} = S/C = (2\pi\kappa/\alpha)^{1/2}, \tag{6}$$

the thickness of the sheet may be best defined as $d \equiv (2\pi\kappa/\alpha)^{1/2}$.

It is notable that, by differentiating Eq. (2) with respect to x_1, we obtain the equation for the one-dimensional (1D) Burgers vorticity field in the same stagnant flow [9] only if $\partial T/\partial x_1$ is considered as the vorticity in the x_2 direction. Thus, our exact solution for the scalar-gradient sheet is mathematically equivalent to that for the 1D Burgers vorticity layer.

3. Working postulates

Here we explain some necessary postulates for considering the statistics of the sheets in turbulent fluid.

Postulate 1. The multifractal structure of scalar dissipation is derived from the tetranomial Cantor set model as a joint multifractal measure for both energy and scalar dissipations.

Meneveau et al. [10] were the first to describe the distribution of scalar dissipation in terms of a joint multifractal measure for both energy and scalar dissipations, even though it was developed in a 1D cut of space in order to compare with their 1D experimental data series. This idea is reasonable, since the scalar is advected by the turbulent velocity field so that a complicated spatial arrangement of the scalar must be somehow linked to that of the latter, which is characterized by the multifractal structure of energy dissipation. The tetranomial Cantor set model developed in 3D space by the present author [7,8] improved the idea in a more generalized and satisfactory way in view of comparison of the ever (but slowly) increasing scaling indices of scalar structure functions with experiment. No more powerful model has been contrived so far. There has been a discussion on the tendency of the scaling indices that they may saturate to a certain constant asymptotically [11], but it can not be considered as universal or realistic because the base of the discussion is a DNS of two-dimensional turbulence; even though this paper [11] clarified the importance of scalar-gradient sheets in turbulence by the name of fronts or cliffs.

In this model [7,8], both energy and scalar dissipations serve as a joint multifractal measure in 3D space in the inertial-convective scaling range, that is, the range from macroscale L down to the larger of Kolmogorov scale η and its counterpart for the advected scalar, η_S $(= (\kappa^3/\varepsilon)^{1/4})$. If $L > l > r > \mathrm{Max}(\eta, \eta_S)$ and we write energy and scalar dissipations locally averaged over a domain of scale r as ε_r (therefore $\varepsilon = \varepsilon_L$) and χ_r, respectively, then the stochastic variable $y = \varepsilon_r/\varepsilon_l$ and $z = \chi_r/\chi_l$, where the domain of scale r in question should be involved in the domain of scale l, distribute themselves spatially with the joint PDF:

$$p(y,z;r/l) = \sum_k {}_\Omega C_k A^k (1/2 - A)^{\Omega - k} \sum_{l,m} {}_k C_{l\Omega - k} C_m \times \delta(y - B^{l+m} C^{\Omega - l - m}) \delta(z - D^l E^{k-l} F^m G^{\Omega - k - m}). \tag{7}$$

The parameters B, C and Ω are fixed by the binomial Cantor set for energy dissipation measure in turbulence, since $\int p\,\mathrm{d}z$ should reduce to the PDF of y for turbulence without a passive scalar (that is $2^{-\Omega} \sum_k {}_\Omega C_k \delta(y - B^k C^{\Omega - k})$ [5]). Therefore, $\Omega = -\ln(r/l)/\ln A$, $A = 2^{1/3}$ and B,

$C = 1 \pm (2^{\mu/3} - 1)^{1/2}$ (that is, $B = 1.2175$ and $C = 0.7825$ when we take the second-order intermittency exponent $\mu = 0.20$, a currently accepted value). The other parameters newly appear, reflecting a tetranomial Cantor set structure of scalar dissipation measure. The recommended values [7] for them in view of comparison with experiment are $A = 0.156$, $D = 1.067$, $E = 0.358$, $F = 1.20$ and $G = 1.06$.

Particularly for $r/l = 1/2^{1/3}$, we have

$$p(y,z;2^{-1/3}) = A[\delta(y-B)\delta(z-D) + \delta(y-C)\delta(z-E)] + (1/2 - A)[\delta(y-B)\delta(z-F) + \delta(y-C)\delta(z-G)]. \quad (8)$$

Although the present $p(y,z;r/l)$ is relevant to scale ratio r/l of domains in 3D space, the PDF itself would be applicable extensively in other dimensional spaces. However, it should be taken into account that if this PDF is applied in 1D space, the scale ratio must be changed to $(r/l)^{1/3}$. Thus, the present PDF for scale ratio $= 1/2^{1/3}$ really means the PDF at a half splitting in scale occurring only in 1D space. This implies that in a 1D half-splitting process in cascade there are four possible discrete values for z, stochastic measure ratio $\chi_{1/2_{(1/3)}}/\chi_1$, while there are two for y.

Generally speaking, it is an idealization to assume a discrete probability for values of y and z such as in Eqs. (7) and (8). Real phenomena would naturally be described by a continuous probability. However, sometimes they may reveal their essential characters by an extreme simplification of description, only if the results deduced from it well approximate various experimental evidences of the phenomena. Then it offers a really useful method for analyzing a complicated physical process in a relatively simple way. The present joint Cantor set structure model for energy and scalar dissipations must be considered just as such.

Postulate 2. The scalar field across a scalar-gradient sheet in turbulence can be approximately considered as 1D and represented by the exact solution (4) with the same scalar gap.

Even though real gradient sheets in turbulence are never 1D, having a limited width and curvature, this postulate makes it quite easy to handle all the calculation.

We assume that the thickness of the sheet is m_s times the local η_s value in a domain of scale r', that is $\eta'_s = (\kappa^3/\varepsilon'_r)^{1/4} = (\kappa^3/\varepsilon_L)^{1/4} y^{-1/4}$, where $y = \varepsilon'_r/\varepsilon_L$; r' is the smallest scale over which we can consider the local character of turbulence and which should involve the whole inertial range of scale. As a result, we have

$$d/\eta_s = m_s y^{-1/4}. \quad (9)$$

In this paper we will take $r' = L/8$ in the same thought as we did for the statistics of worms in turbulence [5] previously, and $m_s = 4$, which is a plausible value to our knowledge in all the DNS performed on the thickness so far [1–4]. The choice of $m_s = 4$ has been recently supported by experiment [12], which states that the mean thickness of sheets $\cong 13\eta$ follows a $R_\lambda^{-3/2}$ scaling. While it is obvious that η has a $R_\lambda^{-3/2}$ scaling [13], the mean width becomes about 3.4 η_s, if the Pr based on $\nu = 2.8 \times 10^{-4}$ cm^2/s and $\kappa = 17 \times 10^{-4}$ cm^2/s in the paper is taken into consideration (that is, if divided by $(\kappa/\nu)^{3/4}$). Here if the average is taken with the PDF of y, the mean of d in (9) is very close to that value. This can be well understood from the Fig. 2(a) in Appendix A, which shows the PDF of d/η_s.

We can calculate χ_d at the middle of the sheet, using Eq. (3), as

$$\chi_d = \kappa \int_{-d/2}^{d/2} (\partial T/\partial x_1)^2 \mathrm{d}x_1/d = \kappa C^2 (\pi\kappa/\alpha)^{1/2} \mathrm{Erf}[(\alpha/\kappa)^{1/2} d/2]/d. \quad (10)$$

Taking only the first term of the formula: $\mathrm{Erf}[z] = \frac{2}{\sqrt{\pi}} \mathrm{e}^{-z^2}(z + \frac{2}{3}z^3 + \ldots)$ since d is a small value, we have

$$\chi_d = \kappa C^2 \mathrm{e}^{-\pi/2} = \kappa S^2 \mathrm{e}^{-\pi/2}/d^2,$$

or

$$S = (\mathrm{e}^{\pi/4} d/\kappa^{1/2}) \chi_d^{1/2}. \quad (11)$$

Postulate 3. The spatial distribution of scalar dissipation near a scalar-gradient sheet must be locally almost 1D.

This is consistent with the exact solution explained in the preceding section and compares well with the numerically observed sheet structure of concentrated scalar dissipation regions. But this Postulate puts a strong restriction on the application of Postulate 1 to a domain of small scale, at least, less than Taylor-scale. For such scales, the half-splitting in the measure breakdown process of Postulate 1 should be interpreted one-dimensionally, that is, as the splitting of a plate into two thinner half plates.

Thus, we take a simple idealization that a Taylor-scale ($= \lambda$) wide cube splits into λ/d plates each d thick and λ wide, after such a half-splitting process is repeated n times; $n = \log_2(\lambda/d)$. Only a plate with the maximum measure ratio $z = F$ (in Eq. (8)) among a pair of two plates which have occurred in the final breakdown process can form a scalar-gradient sheet, if the measure there makes a local maximum. In order for the measure to be locally maximum, the measure ratios in the one step preceding to final splitting are relevant. We have

three cases to be considered. If the measure ratio is F in this splitting, too, the measure at the plate in question is always a local maximum; the probability that such a case occurs is $(1/2-\Lambda)^2$ as is obvious from Eq. (8). If it is D, the plate in question has a locally maximum measure only unless the measure ratio of the other plate in that splitting is F and the measure ratio arising from the splitting of this plate is D or F; the probability for this case is $\Lambda(1/2-\Lambda)[1-(1/2-\Lambda)(\Lambda+1/2-\Lambda)]$. Finally, if it is G, the plate in question has a local maximum measure if the measure ratio of the other plate in that splitting is F with E as the measure ratio arising from the splitting of this plate, if the same is D with D, G or E and if the same is E with F, D, G or E; the probability for this case is $(1/2-\Lambda)^2\{(1/2-\Lambda)\Lambda+\Lambda[\Lambda+(1/2-\Lambda)+\Lambda]+\Lambda\}$. To sum up all these probabilities, we have $(1/2-\Lambda)(1/2+3\Lambda/4-3\Lambda^2/2)$ as the probability that one of the plates in the final splitting is a sheet with a local maximum of scalar dissipation. That is 0.200 for the value of $\Lambda=0.156$. It means that 20.0% of the λ/d plates can be the sheets.

This idealization may be an extreme modeling. In fact, such an orderly alignment of scalar-gradient sheets in a Taylor-scale wide cube is hardly ever observed exactly. What we can expect to see is an entanglement of more or less deformed sheets, keeping the same topology as the straight parallel plates assumed above in the cube. This expectation looks reasonable, however, since our multifractal assumption in Postulate 1 already designates a possible spatial distribution of scalar dissipation over the entire inertial-convective range of scale, and since its reality was evidenced by the scaling of scalar structure functions [7] and the PDF of scalar increment for various scales [8]. Therefore, even the PDF of scalar dissipation in a 1D structure of fine scale cannot be free from the form given by Eq. (7), and is considered to be treated by the same PDF (but with the modified scale ratio noted in Postulate 1).

Thus, we have the expression of scalar dissipation in a sheet which is the plate with $z=F$ in the final breakdown process,

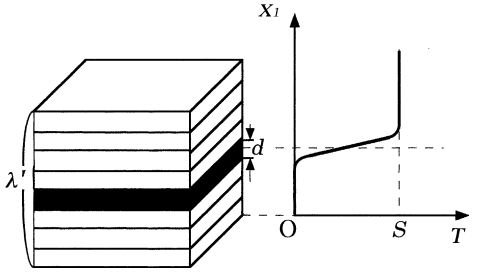

Fig. 1. Schematic sketch of a sheet (black region) with local maximum of $\chi_d(=$ e.g. $FF\cdots F\chi\lambda')$ in a cube of side length λ'. The corresponding profile of the passive scalar in the x_1 axis is shown on the right-hand side.

$$\chi_d = F(\chi_{\lambda(1/2)^{(n-1)/3}}/\chi_\lambda)(\chi_\lambda/\chi_{r'})(\chi_{r'}/\chi_L)\chi_L, \tag{12}$$

together with Eq. (8) and the remark there (on application of the PDF in another space dimension) in mind. We shall introduce a local Taylor-scale λ' in place of λ in the later sections, like a local η_s scale, which depends on y. A schematic sketch of the sheet structure based on these postulates is given in Fig. 1. Of course, there may be more than one sheet in a cube of side length λ'.

4. Number, area and volume of scalar-gradient sheets

Now let us calculate the number of sheets with the thickness d within the volume of $L^3, N(d)$. Postulate 3 gives directly

$$N(d) = 0.200(\lambda'/d)(L^3/\lambda'^3), \tag{13}$$

where λ' is the local Taylor-scale, which is related to $\varepsilon_{r'}$ by $\lambda'^2\varepsilon_{r'} = \lambda^2\varepsilon_L(=15\nu\langle u^2\rangle; \langle u^2\rangle$: square-average of longitudinal velocity fluctuation [13]). After taking into account Eq. (9), $\eta/L \cong 15^{3/4}R_\lambda^{-3/2}$ and $\lambda/L \cong 15R_\lambda^{-1}$ [13], and putting $y=\varepsilon_{r'}/\varepsilon_L$, Eq. (13) can be rewritten as

$$N(d) = 0.200/(15^{11/4}m_s)y^{5/4}R_\lambda^{7/2}Pr^{3/4}, \tag{14}$$

where $Pr=\nu/\kappa$. We should here note from Eq. (9)

$$y = m_s^4(d/\eta_s)^{-4}(=m_s^4(d/\eta)^{-4}Pr^{-3}). \tag{15}$$

Eq. (14) shows that $N(d)$, which is stochastic in y, and the total number of sheets, which is the average of $N(d)$, are in proportion to $R_\lambda^{7/2}$ and $Pr^{3/4}$, since the scale $r'(=L/8)$ to govern the PDF of y is considered to be independent of R_λ and Pr, as assumed in Postulate 2.

The total number of sheets in a macroscale box of volume L^3 is given as the expectation value of Eq. (14):

$$N_T = 0.200/(15^{11/4}m_s)R_\lambda^{7/2}Pr^{3/4}\int\int y^{5/4}p(y,z;r'/L)\,dy\,dz. \tag{16}$$

Since $\int\int y^{5/4}\,p(y,z;r'/L)\,dy\,dz = [(B^{5/4}+C^{5/4})/2]^9 = 1.069$ (with $r'/L=1/8$) we have 1288 sheets for $R_\lambda=150$ and $Pr=1$. The standard deviation is calculated as $1.002N_T$ from the value of $\int\int y^{5/2}p(y,z;r'/L)\,dy\,dz = [(B^{5/2}+C^{5/2})/2]^9 = 2.147$.

The total area of sheets is very important for mixing process as well as reaction process of the scalar. Since a sheet is λ' wide, it is calculated as the expectation value of $\lambda'^2N(d)$:

$$0.200L^2/(15^{3/4}m_s)R_\lambda^{3/2}Pr^{3/4}\int\int y^{1/4}p(y,z;r'/L)\,dy\,dz$$
$$= 0.200L^2/(15^{3/4}m_s)R_\lambda^{3/2}Pr^{3/4}[(B^{1/4}+C^{1/4})/2]^9, \tag{17}$$

which is in proportion to $R_\lambda^{3/2}$ and $Pr^{3/4}$. For example, all sheets cover an area of 11.6 times L^2 in case of $R_\lambda = 150$ and $Pr = 1$. Here is a secret of the great turbulence power for scalar transport phenomenon.

If we express d from Eq. (15), we have

$$d = m_s Pr^{-3/4} y^{-1/4} \eta = 15^{3/4} m_s R_\lambda^{-3/2} Pr^{-3/4} L y^{-1/4}. \tag{18}$$

This gives rise to

$$d\lambda'^2 N(d) = 0.200 L^3, \tag{19}$$

which is invariant to y. Hence we may understand that the volume of sheets is not stochastic and always occupies 20.0% of the total volume of fluid, irrespective of R_λ and Pr. It is apparent that this ratio stems directly from Postulate 3.

5. Scalar transfer rate in turbulence and Nusselt number

The total scalar transfer Tr in a macroscale volume in turbulence per unit time may be estimated as the expectation value of

$$(\kappa S/d)\lambda'^2 N(d) = 0.200 \mathrm{e}^{\pi/4}/(15^{3/4} m_s) \times (\kappa \chi_L F)^{1/2} R_\lambda^{3/2} Pr^{3/4} L^2 (z'' z')^{1/2} y^{1/4}, \tag{20}$$

that is obtained by using Eqs. (11), (12) and (17). The stochastic part, $(z'' z')^{1/2} y^{1/4}$, has only to be averaged with a combined PDF: $p(y'', z''; 1/2^{(n-1)/3}) p(y', z'; 120/(R_\lambda y^{1/2})) p(y, z; 1/8)$. This calculation is analytically possible if Eq. (7) is used. In fact, the first double integral $\int\int z''^{1/2} p \, \mathrm{d}y'' \mathrm{d}z''$ reduces, by taking $\Omega = -\ln(1/2^{(n-1)/3})/\ln A = n - 1$, to

$$\begin{aligned} &\sum_k {}_\Omega C_k \Lambda^k (1/2 - \Lambda)^{\Omega - k} \\ &\quad \times \sum_{l,m} {}_k C_l \, {}_{\Omega-k} C_m D^{1/2} E^{(k-l)/2} F^{m/2} G^{(\Omega - k - m)/2} \\ &\quad = [\Lambda (D^{1/2} + E^{1/2}) + (1/2 - \Lambda)(F^{1/2} + G^{1/2})]^\Omega \\ &\quad = [(15^{1/4}/m_s) R_\lambda^{1/2} Pr^{3/4} y^{-1/4}/2]^{(4\gamma - 1)/5}, \end{aligned} \tag{21}$$

where we have put $(4\gamma - 1)/5 = \log_2[\Lambda(D^{1/2} + E^{1/2}) + (1/2 - \Lambda)(F^{1/2} + G^{1/2})]$. The second double integral $\int\int z'^{1/2} p \, \mathrm{d}y' \mathrm{d}z'$ is carried out in the same way, by taking $\Omega = -\ln[120/(R_\lambda y^{1/2})]$, as

$$\begin{aligned} &[\Lambda (D^{1/2} + E^{1/2}) + (1/2 - \Lambda)(F^{1/2} + G^{1/2})]^\Omega \\ &\quad = [120/(R_\lambda y^{1/2})]^{-3(4\gamma - 1)/5}. \end{aligned} \tag{22}$$

The third double integral with respect to y and z contains the stochastic factor $y^\gamma z^{1/2}$, to which Eqs. (21) and (22) have contributed, and that is integrated as

$$\begin{aligned} &\int\int y^\gamma z^{1/2} p(y, z; 1/8) \, \mathrm{d}y \, \mathrm{d}z \\ &\quad = [\Lambda (B^\gamma D^{1/2} + C^\gamma E^{1/2}) + (1/2 - \Lambda)(B^\gamma F^{1/2} + C^\gamma G^{1/2})]^9. \end{aligned} \tag{23}$$

The prefactor remaining from Eqs. (21) and (22) amounts to

$$R = [15^{1/4}/(2m_s)]^{(4\gamma - 1)/5} 120^{-3(4\gamma - 1)/5} R_\lambda^{7(4\gamma - 1)/10} Pr^{3(4\gamma - 1)/20}. \tag{24}$$

Thus, the product of Eqs. (23) and (24) gives the expectation value of the stochastic part wanted.

In our multifractal model explained in Postulate 1, we have $(4\gamma - 1)/5 = -0.02089$, and then $\gamma = 0.2239$, so that the right-hand side of Eq. (23) becomes 0.8803. Combining this, R and the other part of Eq. (20) altogether (with $m_s = 4$), we have the final formula:

$$Tr = 0.0216 (\kappa \chi_L)^{1/2} R_\lambda^{1.427} Pr^{0.734} L^2. \tag{25}$$

Thus, apart from the factor $(\kappa \chi_L)^{1/2}$, the efficiency of turbulent mixing may be said to increase almost in proportion to $R_\lambda^{3/2} Pr^{3/4}$; even though the actual power exponents are slightly smaller, affected by the factor R in Eq. (24).

The factor $(\kappa \chi_L)^{1/2}$ may be reformed, using the concept of scale-similar scalar cascade in the inertial-convective range of scale that implies

$$\chi_L = \langle (T - \langle T \rangle)^2 \rangle \langle u^2 \rangle^{1/2} / L \tag{26}$$

to be $(PrRe)^{1/2} \kappa \langle (T - \langle T \rangle)^2 \rangle^{1/2}/L$ where $Re = \langle u^2 \rangle^{1/2} L/\nu$. If we rewrite (25) using this and the relation: $R_\lambda = (15Re)^{1/2}$, we have

$$Tr = 0.00558 R_\lambda^{2.427} Pr^{1.234} L^2 \kappa \langle (T - \langle T \rangle)^2 \rangle^{1/2} / L \tag{27}$$

or

$$Tr = 0.149 \mathrm{Re}^{1.214} Pr^{1.234} L^2 \kappa \langle (T - \langle T \rangle)^2 \rangle^{1/2} / L. \tag{28}$$

Since $\langle (T - \langle T \rangle)^2 \rangle^{1/2}$ is considered as a representative value of macroscale variation of scalar T, the factor $\langle (T - \langle T \rangle)^2 \rangle^{1/2}/L$ in (27) should be interpreted as comparable with a scalar gradient really observable over scale L in this turbulence. Thus, the right-hand side of Eq. (27) is the same as the scalar transfer rate, obtained when we have a scalar gradient $\langle (T - \langle T \rangle)^2 \rangle^{1/2}/L$ normal to the cross-section of area L^2, in a fluid with the scalar diffusion coefficient:

$$\kappa_T = (0.00558 R_\lambda^{2.427} Pr^{1.234} \text{or } 0.149 Re^{1.214} Pr^{1.234}) \text{times } \kappa. \tag{29}$$

This new coefficient κ_T implies an enormous gain in diffusivity in comparison with κ (and may be called

turbulent diffusion coefficient), which would be usable for sketching the outer-macroscale process of turbulent diffusion under the assumption of fully-developed isotropic turbulence existing in inner scales.This is the first theoretical prediction of the turbulent diffusion coefficient in isotropic turbulence. It is an important target which has long been awaited to be achieved from an engineering practical point of view, since the mathematical concept of multifractal applied to turbulence was advocated many years ago [1,6,7,10,14–16]. The scaling of κ_T is, after all, close to $R_\lambda^{5/2}Pr^{5/4}$ or $Re^{5/4}Pr^{5/4}$, which necessarily comes from our multifractal sheet model of scalar gradient and the traditional concept of energy and scalar cascades in the inertial-convective range of scale in high-Reynolds number turbulence.

The quantity $\kappa_T/\kappa = 0.149Re^{1.214}Pr^{1.234}$ obtained from (29) may be understood to be the Nusselt number Nu of scalar transfer over a macroscale L from a plate in contact with a homogeneous isotropic turbulent fluid, only if the turbulence is kept isotropic. However, the presence of mean scalar gradient, in itself, necessarily causes a statistical anisotropy even if slightly. Then, it may be hard to predict very exactly from our theory real Nusselt numbers in various anisotropic turbulent flows containing an advected scalar. Let us compare our prediction with the experiment of Jayesh and Warhaft [17] who used a grid-generated decaying homogeneous turbulence with a mean vertical temperature gradient imposed. Their formula is $Nu = 0.73Re^{0.88}$ with $Pr = 0.7$ for the range of $60 < Re < 1100$. This gives $Nu = 76$ and 132 for $Re = 197$ and 369, respectively, while we have $\kappa_T/\kappa = 59$ and 125 for the same Re and Pr. There is an appreciable difference between the corresponding values in both cases, but it seem to be acceptable, if both a possible experimental error and an extreme idealism inherent to our mathematical theory are taken into account.

Our theory, however, would be more relevant to a higher-Re turbulence with a very wide inertial-convective range involving deep cascades of energy and scalar. The higher exponent of Re in κ_T/κ seems to indicate this feature. The ultimate value of the exponent in turbulent scalar advection is still unfixed. It may be added, however, that the exponent of Nusselt number would reach 1 in a turbulent Rayleigh–Benard convection for (very high Rayleigh numbers and so) high Reynolds numbers; that is, $Nu \sim RePr$, according to the recent work of Lohse and Toschi [18]. (Note that thermally-forced turbulence in the Rayleigh–Benard flow is considered to be nearly isotropic except very near the top and bottom surfaces for very high Rayleigh numbers.) It is to be further noted that there is a constraint for two parameters R_λ and Pr to guarantee the validity of our theory such that $R_\lambda^{1/2}Pr^{3/4} > 2m_s/15^{1/4}$, as described in Appendix B; for Pr small, R_λ must be large enough.

Thus, these comparisons would signify that our idealistic view of advected scalar turbulence on the multifractal basis has a substantial reality or practicability. However, it may be the most direct method of identifying κ_T to observe, by any means, how rapidly a contaminant from a point source expands through an isotropically turbulent fluid; since the contaminant must diffuse statistically over a macroscale length, obeying a parabolic differential equation with κ_T as diffusion coefficient. This is free from an imposed mean scalar gradient which affects the statistical isotropy of turbulence more or less.

6. Conclusion

It is an essential property of an advected scalar that its gradient forms a huge number of sheets in high Reynolds number turbulence, and this provides a great advantage for scalar mixing or reaction process. Based on the three Postulates, we have phenomenologically predicted the statistical structure of these sheets distributed in a turbulent fluid. In other words, the tetranomial Cantor set model for isotropic turbulence with an advected scalar, that implies a special joint scale-similarity or multifractality (in the inertial-convective range) of cross dissipation measure in $y \times z$ space, together with the exact solution of the advected scalar equation representing the sheet, has revealed itself as a useful tool in dealing with the nature of advected scalar turbulence, at least, qualitatively. In particular, an explicit formula of turbulent diffusivity in fully-developed isotropic turbulence has been derived on this basis, and the macroscale scalar transfer predicted from this has been fairly compared with the heat transfer across a grid-generated homogeneous turbulence in the presence of mean vertical temperature gradient [17].

Appendix A. PDFS of the thickness and width of sheets

We know from Eq. (15) that the thickness d of a sheet is stochastic according to the PDF of y. Then we have the PDF of d in the normalized form as

$$P(d/\eta_s) = 4m_s^4(d/\eta_s)^{-5}y^{5/4} \times \int p(y,z;r'/L)\,\mathrm{d}z \Big/ \int\int y^{5/4}p(y,z;r'/L)\,\mathrm{d}y\mathrm{d}z, \tag{A.1}$$

together with Eq. (15). It is remarkable that the PDF is independent of R_λ and Pr, so long as d is normalized by η_s. $\int p(y,z;r/l)\,\mathrm{d}z$ is nothing but the binomial Cantor set model for energy dissipation measure, as is noted in Postulate 1. The $p(y,z;r/l)$ in our model is basically a multinomial delta function in $y \times z$ space, which implies a probability on a discrete set in the space. And so is $\int p(y,z;r/l)\,\mathrm{d}z$ in y space. However, we can relax this limited situation for the case of the binomial Cantor set

model to let the PDF imply a probability on a continuous set in y space by taking the step-function approximation, which was explained in the previous paper [5], to simulate $\int p(y,z;r/l)\,\mathrm{d}z$. The $P(d/\eta_s)$ obtained using this approximation to $\int p(y,z;r'/L)\,\mathrm{d}z$, is shown in Fig. 2(a). ($m_s = 4, r'/L = 1/8$, and $\mu = 0.2$ are the values according to the postulates.) The associated smooth curve in the figure is the case in which we have replaced $\int p(y,z;r/l)\,\mathrm{d}z$ by the lognormal model of Kolmogorov: $p_L(y;r/l)$, that is,

$$p_L(y;r/l) = \exp\{-[\ln y - m(r/l)]^2/[2s(r/l)^2]\}/[(2\pi)^{1/2} y s(r/l)]$$

with

$$s(r/l) = [\mu \ln(l/r)]^{1/2}, \quad m(r/l) = -s(r/l)^2/2. \tag{A.2}$$

Hence we can see that the lognormal approximation to $\int p(y,z;r/l)\,\mathrm{d}z$ is almost equally good for the calculation of $P(d/\eta_s)$. The previous paper [5] showed how well $p_L(y;r/l)$ approximates $\int p(y,z;r/l)\,\mathrm{d}z$ itself for various r/l. These approximations to the discrete function in y space may be understood as a kind of coarse graining (in y space) which is familiar in statistical mechanics. The Fig. 2(a) is substantially supported by the experiment [12], which gives the mean of $d \cong 13\eta$, as is described in the text.

A scalar-gradient sheet is considered to have the width of local Taylor-scale λ', from the DNS observation. Then, the PDF for a sheet to have width λ', when it is normalized by λ, is given in a similar way as

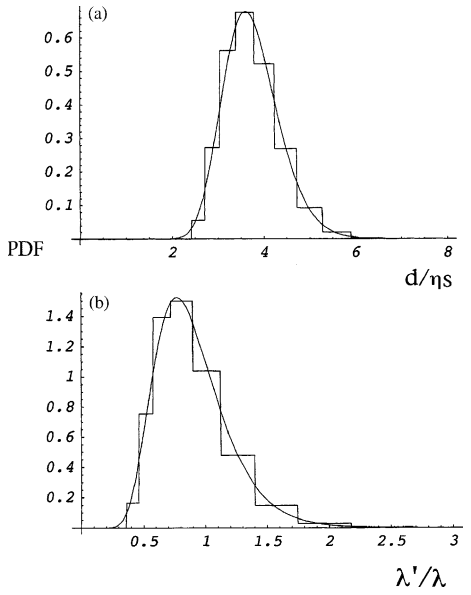

Fig. 2. The PDFs of thickness (normalized by η_s) (a) and width (normalized by λ) (b) of a sheet; based on the step-function approximation and lognormal approximation.

$$P(\lambda'/\lambda) = 2(\lambda'/\lambda)^{-3} y^{5/4} \times \int p(y,z;r'/L)\,\mathrm{d}z \Big/ \int\int y^{5/4} p(y,z;r'/L)\,\mathrm{d}y\mathrm{d}z, \tag{A.3}$$

only if the relation:

$$y = (\lambda'/\lambda)^{-2} \tag{A.4}$$

is taken into account. Fig. 2(b) shows the $P(\lambda'/\lambda)$ calculated using the same step-function approximation to $\int p(y,z;r'/L)\,\mathrm{d}z$. The associated smooth curve is the result obtained by the same lognormal approximation to $\int p(y,z;r'/L)\,\mathrm{d}z$.

By the way, it may be noted that we can also find the PDF of the strain α in a sheet, since $\alpha = 2\pi\kappa/d^2$ by definition and we already know the PDF of d.

Appendix B. PDF of scalar gap across a sheet

From Eqs. (11) and (12) we may express the scalar gap normalized by $(\kappa^{1/4}\chi_L^{1/2}/\varepsilon_L^{1/4})$ as

$$S/(\kappa^{1/4}\chi_L^{1/2}/\varepsilon_L^{1/4}) = \mathrm{e}^{\pi/4} m_s (Fz''z'z)^{1/2} y^{-1/4}, \tag{B.1}$$

where we have put $z = \chi_{r'}/\chi_L$, $z' = \chi_{\lambda'}/\chi_{r'}$ and $z'' = \chi_{\lambda'(1/2)^{(n-1)/3}}/\chi_{\lambda'}$. According to Postulate 3, n is given as

$$n = \log_2(\lambda'/d) = \log_2[(15^{1/4}/m_s) R_\lambda^{1/2} Pr^{3/4} y^{-1/4}], \tag{B.2}$$

after taking into account Eq. (15) and $\lambda/\eta = 15R_\lambda^{1/2}$ [13].

Since we know the PDF of y, z, z', z'' by means of Postulate 1, the PDF of $S/(\kappa^{1/4}\chi_L^{1/2}/\varepsilon_L^{1/4}) \equiv \Sigma$ can be formulated as

$$P(\Sigma) = 2\Sigma \int\int\int 1/(a^2 z' z y^{-1/2}) \times \int p(y'', \Sigma^2/(a^2 z' z y^{-1/2}); 1/2^{(n-1)/3})\,\mathrm{d}y'' \times \int p(y', z'; 120/(R_\lambda y^{1/2}))\,\mathrm{d}y'\mathrm{d}z' p(y,z;1/8)\,\mathrm{d}y\mathrm{d}z, \tag{B.3}$$

where $a = \mathrm{e}^{\pi/4} m_s F^{1/2}$. It is to be noted that y and z are correlated with each other but z' and z'' are independent fragmentations in our multifractal model. Since the parameter r/l in $p(y,z;r/l)$ must be less than 1 in order for a fragmentation of the measure to occur, our formulation requires that $n > 1$, i.e. $R_\lambda^{1/2} Pr^{3/4}$ be larger than $2m_s y^{1/4}/15^{1/4}$, and that $120/(R_\lambda y^{1/2}) < 1$. When $n \leqslant 1$, no fragmentation can occur, so it is suitable to simply set $\int p(y'', z'')\,\mathrm{d}y'' = \delta(z'' - 1)$. For the same reason, we put $\int p(y', z')\,\mathrm{d}y' = \delta(z' - 1)$ for $120/(R_\lambda y^{1/2}) \geqslant 1$.

$P(\Sigma)$ is a discrete function because $p(y,z;r/l)$ in Eq. (7) is a discrete function. Unfortunately there is no simple-shape approximations to $p(y,z;r/l)$ and even $\int p(y,z;r/l)\,\mathrm{d}y$ such that they could represent suitable

measures on continuous sets in $y \times z$ and z space, respectively. This is a situation in big contrast to $\int p(y,z;r/l)\,\mathrm{d}z$ which has the step-function or lognormal approximation described in the preceding section. As a result, the probabilities at various discrete points of Σ generally scatter in a very complicated way. Therefore it is most suitable to represent $P(\Sigma)$ by a normalized histogram in order to grasp a global trend for the PDF of Σ. This may be considered as another kind of coarse graining (in Σ space).

We can see such a histogram in Fig. 3 for $Pr = 1$ and various values of R_λ. The height of each column in the histogram indicates the sum of the probabilities of all the discrete points of Σ involved in the respective column with unity band width, so that the total area of the histogram should be exactly unity, as easily understood from Eqs. (7) and (B.3). As R_λ gets large, the number of discrete points of Σ increases in each column, but it is not likely that a substantial change in the global PDF pattern of Σ appears, at least, until $R_\lambda = 4000$. A remarkable thing seen here is that the PDF is not of a simple bell-type but has three or more lumps; the highest peak among the lumps is located near $\Sigma = 9$ and the next one is near $\Sigma = 5$ until $R_\lambda = 1000$. But at $R_\lambda = 4000$ the peak near $\Sigma = 9$ gets lower while the lump near $\Sigma = 5$ has the highest peak.

For Pr larger than 1 and $R_\lambda = 150$, the number of discrete points in the histogram increases with Pr and the lumps of $P(\Sigma)$ considerably shift toward higher values of Σ, as is seen in Fig. 4. In this case, the highest peak is always in the middle lump. It is noted in Fig. 4(b) for $Pr = 100$, however, that a new lump grows with a high peak near $\Sigma = 4$.

For Pr smaller than 1 and $R_\lambda = 1000$, the above-described tendency that the lumps of $P(\Sigma)$ shift toward higher values of Σ with increasing Pr is invariant, as is seen from Fig. 5. But the highest peak is always in the rightest lump. The distribution pattern of lumps is rather similar to those in Fig. 3. It is noted in Fig. 5(c) for $Pr = 0.1$, however, that the third lump vanishes entirely. For a small Pr, R_λ must be large enough to insure the condition $R_\lambda^{1/2} Pr^{3/4} > 2m_s/15^{1/4}$; otherwise, η_s would absurdly surpass Taylor-scale λ (from the viewpoint of inertial-convective scale-range).

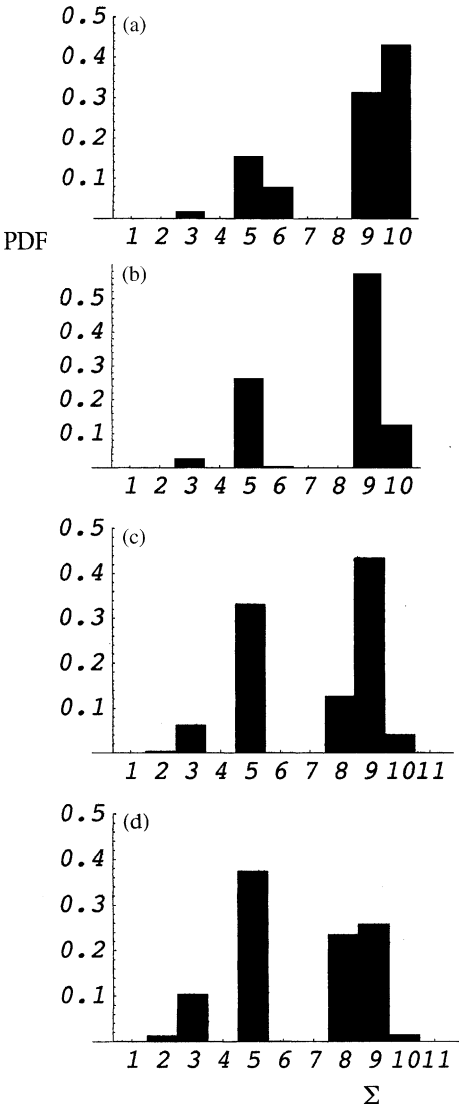

Fig. 3. The PDF of scalar gap (normalized by $\kappa^{1/4}\chi_L^{1/2}/\varepsilon_L^{1/4}$) across a sheet for $Pr = 1$ and for $R_\lambda = 150$ (a), 300 (b), 1000 (c) and 4000 (d).

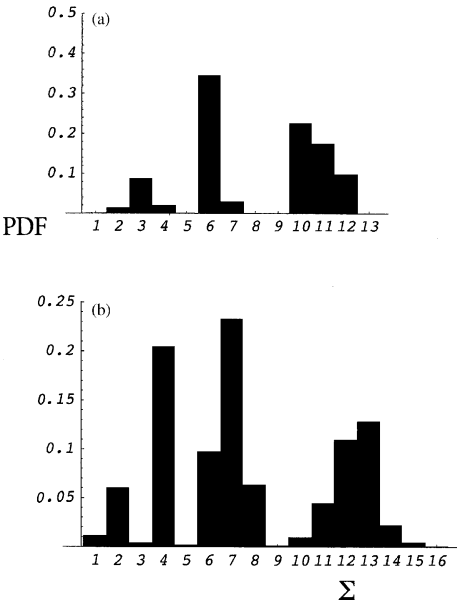

Fig. 4. The PDF of scalar gap (normalized by $\kappa^{1/4}\chi_L^{1/2}/\varepsilon_L^{1/4}$) across a sheet for $R_\lambda = 150$ and for $Pr = 10$ (a) and 100 (b).

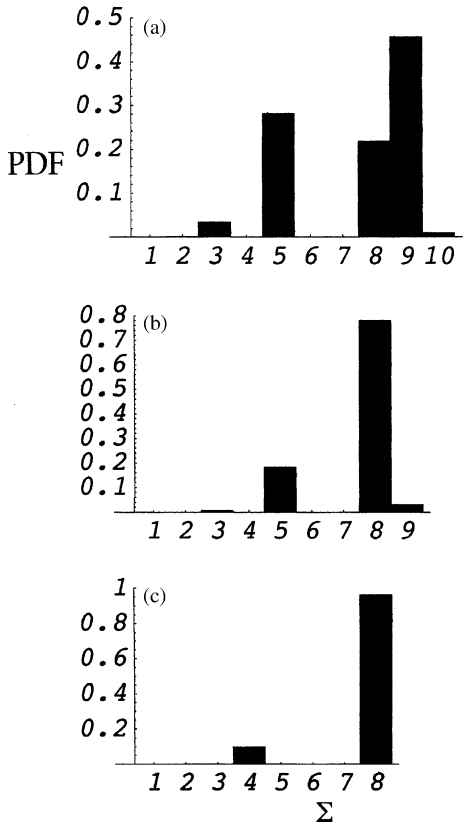

Fig. 5. The PDF of scalar gap (normalized by $\kappa^{1/4}\chi_L^{1/2}/\varepsilon_L^{1/4}$) across a sheet for $R_\lambda = 1000$ and for $Pr = 0.5$ (a), 0.2 (b) and 0.1 (c).

All these features of $P(\Sigma)$ predicted by our treatment look novel but a necessary result from the theory. How close to reality they are must be eventually judged by comparison with a DNS or experiment in future. This will be a crucial test of the present theory on whether the joint multifractal measure in it could represent the qualitative essence of passive scalar turbulence.

All the calculations of the PDFs in Eqs. (A.1), (A.3) and (B.3) were carried out with the help of "Mathematica 3.0" by Wolfram.

References

[1] I. Hosokawa, S. Oide, K. Yamamoto, Morphological analysis of decaying isotrophic turbulence with a passive scalar, Nagare 17 (1998) 28–44;
Advected scalar version of the differences between the true dissipation and its one-dimensional surrogate in isotropic turbulence, J. Phys. Soc. Jpn. 67 (1998) 1830–1833.

[2] M. Tanahashi, S. Iwase, A.M. Uddin, N. Takata, T. Miyauchi, Distribution of coherent fine scale eddies and turbulent heat transfer in homogeneous isotropic turbulence, Thermal Sci. Eng. 8 (2000) 29–39.

[3] G.R. Ruetsch, M.R. Maxey, Small-scale features of vorticity and passive scalar fields in homogeneous isotropic turbulence, Phys. Fluids A 3 (1991) 1587–1597.

[4] G.R. Ruetsch, M.R. Maxey, The evolution of small-scale structures in homogeneous isotropic turbulence, Phys. Fluids A 4 (1992) 2747–2760.

[5] I. Hosokawa, Statistics of "Worms" in isotropic turbulence treated on the multifractal basis, J. Stat. Phys. 99 (2000) 783–798.

[6] I. Hosokawa, Turbulence models and probability distributions of dissipation and relevant quantities in isotropic turbulence, Phys. Rev. Lett. 66 (1991) 1054–1057.

[7] I. Hosokawa, Temperature structure functions in isotropic turbulence, Phys. Rev. A 43 (1991) 6735–6739.

[8] I. Hosokawa, Probability distribution function of the temperature increment in isotropic turbulence, Phys. Rev. E 49 (1994) 4775–4778.

[9] P.G. Saffman, Vortex Dynamics, Cambridge University Press, Cambridge, 1992, p. 265.

[10] C. Meneveau, K.R. Sreenivasan, P. Kailasnath, M.S. Fan, Joint multifractal measures: theory and applications to turbulence, Phys. Rev. A 41 (1990) 894–913.

[11] A. Celani, A. Lanotte, A. Mazzino, M. Vergassola, Fronts in passive scalar turbulence, Phys. Fluids 13 (2001) 1768–1783.

[12] F. Moisy, H. Willaime, J.S. Andersen, P. Tabeling, Passive scalar intermittency in low temperature helium flows, Phys. Rev. Lett. 86 (2001) 4827–4830.

[13] For example, see H. Tennekes, J.L. Lumley, A First Course in Turbulence, MIT Press, Cambridge, MA, 1972.

[14] I. Hosokawa, K. Yamamoto, Intermittent structure of dissipation in isotropic turbulence viewed from a direct simulation, in: O. Metais, M. Leisure (Eds.), Turbulence and Coherent Structures, Kluwer Academic Publishers, Dordrecht, 1991.

[15] U. Frisch, Turbulence, Cambridge University Press, Cambridge, 1995.

[16] I. Hosokawa, Theory of scale-similar intermittent measures, Proc. R. Soc. London A 453 (1997) 691–709.

[17] Jayesh, Z. Warhaft, Probability distribution, conditional dissipation, and transport of passive temperature fluctuations in grid-generated turbulence, Phys. Fluids A 4 (1992) 2292–2307.

[18] D. Lohse, F. Toschi, Ultimate state of thermal convection, Phys. Rev. Lett. 90 (2003) 034502-1-3.